

Article

Design of 3D Carbon Nanotube Monoliths for Potential-Controlled Adsorption

Dennis Röcker ^{*,†}, Tatjana Trunzer [†], Jasmin Heilingbrunner, Janine Rassloff, Paula Fraga-García  and Sonja Berensmeier ^{*}

Bioseparation Engineering Group, Department of Mechanical Engineering, Technical University of Munich, Boltzmannstraße 15, 85748 Garching, Germany; t.trunzer@tum.de (T.T.); jheilingbrunner91@gmail.com (J.H.); rassloffj@gmail.com (J.R.); p.fraga@tum.de (P.F.-G.)

* Correspondence: d.roecker@tum.de (D.R.); s.berensmeier@tum.de (S.B.)

† These authors contributed equally to this work.

Abstract: The design of 3D monoliths provides a promising opportunity to scale the unique properties of singular carbon nanotubes to a macroscopic level. However, the synthesis of carbon nanotube monoliths is often characterized by complex procedures and additives impairing the later macroscopic properties. Here, we present a simple and efficient synthesis protocol leading to the formation of free-standing, stable, and highly conductive 3D carbon nanotube monoliths for later application in potential-controlled adsorption in aqueous systems. We synthesized monoliths displaying high tensile strength, excellent conductivity (up to 140 S m^{-1}), and a large specific surface area (up to $177 \text{ m}^2 \text{ g}^{-1}$). The resulting monoliths were studied as novel electrode materials for the reversible electrosorption of maleic acid. The process principle was investigated using chronoamperometry and cyclic voltammetry in a two-electrode setup. A stable electrochemical behavior was observed, and the synthesized monoliths displayed capacitive and faradaic current responses. At moderate applied overpotentials ($\pm 500 \text{ mV}$ vs. open circuit potential), the monolithic electrodes showed a high loading capacity ($\sim 20 \mu\text{mol g}^{-1}$) and reversible potential-triggered release of the analyte. Our results demonstrate that carbon nanotube monoliths can be used as novel electrode material to control the adsorption of small organic molecules onto charged surfaces.

Keywords: aqueous system; carbon electrodes; electrosorption; maleic acid; setup design; surface oxidation; ultrasonic technology



Citation: Röcker, D.; Trunzer, T.; Heilingbrunner, J.; Rassloff, J.; Fraga-García, P.; Berensmeier, S. Design of 3D Carbon Nanotube Monoliths for Potential-Controlled Adsorption. *Appl. Sci.* **2021**, *11*, 9390. <https://doi.org/10.3390/app11209390>

Academic Editor: Simone Morais

Received: 20 September 2021

Accepted: 7 October 2021

Published: 10 October 2021

Publisher's Note: MDPI stays neutral with regard to jurisdictional claims in published maps and institutional affiliations.



Copyright: © 2021 by the authors. Licensee MDPI, Basel, Switzerland. This article is an open access article distributed under the terms and conditions of the Creative Commons Attribution (CC BY) license (<https://creativecommons.org/licenses/by/4.0/>).

1. Introduction

Since the discovery of carbon nanotubes (CNTs) by Iijima [1], research interest in these seamless cylindrical graphene layers has been increasing steadily. Due to their outstanding electrical [2], thermal [3], and mechanical properties [4], CNTs are already commercialized for a variety of applications. For instance, in lithium-ion batteries, small quantities of CNTs provide increased electrical conductivity and mechanical stability leading towards an overall enhanced life cycle [5–8]. Nonetheless, CNTs to date are mainly utilized as additives [5–10]. Thus, focussing the extraordinary properties of individual CNTs into macroscopic 3D assemblies still presents a bottleneck on the route to further technical applications [7].

Over the last years, monolith and aerogel synthesis has proven to be a promising way to tune CNTs into macroscopic functional materials [11–15]. CNT monoliths consist of a continuous particle network while simultaneously maintaining the morphological identity of the CNTs [16]. Moreover, these 3D structures are characterized by a large surface area, hierarchical pores, low density, and many accessible active sites for diverse applications [16]. A common approach for monolith synthesis involves gel formation and the subsequent drying out of a particulate suspension of CNTs. Due to the low crosslinking forces between individual CNTs, the efficient dispersion and induction of gelation play

critical roles in monolith synthesis. Therefore, components facilitating the gelation process are often introduced during the synthesis [11–13,15,17–19]. In this context, Kohlmeyer et al. achieved gel formation by using a polymer-based crosslinker [12]. Similarly, Zhang et al. embedded multi-walled carbon nanotubes (MWCNTs) into a polymer matrix [18]. The importance of an initial dispersion of the CNTs has been highlighted by Haghoo et al., who used sodium dodecylbenzene sulfonate (SDBS) for the dispersion of CNTs prior to gelation [15]. However, it has to be considered that these mostly inert additives might alter and impair the later properties of the monolith, as reported by Bryning et al., who reinforced the CNT network with polyvinyl alcohol (PVA) during the monolith synthesis [17]. A first step towards the synthesis of monoliths for technical applications was taken by Shen et al., who focussed on a more economical synthesis protocol using low-cost MWCNTs [11]. While the use of MWCNTs could reduce material costs, the applied protocols in literature still require prolonged time for gelation and special drying techniques such as supercritical fluid drying [11,12,15,17,20]. Thus, the synthesis becomes complex and time-intensive, further reducing the cost-performance ratio of the resulting monoliths [21]. Addressing this research gap, we present a simple and efficient method for synthesizing stable and highly conductive CNT monoliths derived from low-cost bulk MWCNTs. Utilizing ultrasonication for the dispersion and gelation of the CNT suspension and only low amounts of PVA as a stabilizing agent, as well as a simple pressing and heat drying approach, the complexity and time for synthesis can be considerably reduced, enabling a facilitated scale-up and possible technical application of the resulting monoliths.

Many efforts have been made, exploiting the use of CNT-based monoliths as electrode material for supercapacitors or as scaffolds for catalysis [14,22–26]. However, a novel and up-and-coming application alternative presents the targeted electrosorption onto the monoliths' chargeable surface. By applying an electrical potential, the interfacial properties of the monoliths can be tuned in their surface charge and electrical double layer (EDL) structure [27]. Hereby, the adsorption and desorption of ions and molecules can be influenced and steered. In this context, several studies have been published on the use of CNT monoliths for capacitive deionization (CDI) and the removal of inorganic ions from brackish water [24,28,29]. However, the targeted electrosorption of organic molecules onto carbon electrodes is still scarcely studied today.

In a simulative approach, Wagner et al. recently investigated the adsorption equilibria of charged organic molecules at the CNT surface [30]. In view of potential-controlled effects, the electrosorption of small organic molecules on a particulate CNT electrode has been investigated for a chromatographic setup by Trunzer et al. [31,32]. In particular the role of the EDL and the environmental conditions around the solid-liquid interface have been emphasized as critical factors in the electrosorption mechanisms. However, shortcomings of the setup were revealed to be the low electrode capacity and its structural changes throughout the operation time. As a further optimization, the use of a monolithic electrode can increase the mass to volume ratio of the electrode and consequently the number of available binding sites, enable a better and more homogenous potential distribution, and increase the overall structural stability of the electrode.

In the following sections, we characterize: the material properties of untreated and oxidized MWCNTs for monolith synthesis (Section 3.1); the impact of ultrasonication onto the dispersion and gelation of the particle network (Section 3.2); and the resulting monoliths by their macroscopic properties and electrochemically as electrode material (Section 3.3). Moreover, we provide proof of concept for the potential-controlled adsorption and desorption of the small organic molecule maleic acid (Section 3.4). We aim to develop a monolithic electrode for the potential-controlled adsorption of organic molecules as a step ahead to more sustainable and cost-efficient separation processes in biotechnology.

2. Materials and Methods

2.1. Materials and Instruments

MWCNTs were purchased from Future Carbon GmbH (CNT-K, Future Carbon GmbH, Bayreuth, Germany). Prior to monolith synthesis, the particles were washed in 1 M HCl (VWR Chemicals GmbH, Darmstadt, Germany) overnight at 80 °C to reduce the catalytic residue and other contaminants, as suggested by the manufacturer. Surface oxidation of the nanotubes (oxCNTs) was realized in 3 M H₂SO₄ (VWR Chemicals GmbH, Darmstadt, Germany) and HNO₃ (Merck GmbH, Darmstadt, Germany) (ratio 3:1 *v/v*, 30 min, 80 °C) based on the works of Moraes et al. [33] and Shaffer et al. [34]. After oxidation, the nanotube slurry was filtered and thoroughly washed with deionized water (DI-water) until a neutral pH was reached. PVA (89,000–98,000, 99% hydrolyzed, Sigma Aldrich GmbH, Taufkirchen, Germany) was utilized to reinforce the monoliths' structure [11,17,35]. SDBS was purchased from Sigma Aldrich GmbH. Maleic acid (absolute, Ph. Eur., AppliChem GmbH, Darmstadt, Germany) was used as model adsorbate and electrolyte.

Particle characterization was performed with Fourier-transform infrared spectroscopy (FTIR, ALPHA II, Bruker Co., Billerica, MA, USA), transmission electron microscopy (TEM, 100-CX, JEOL GmbH, Freising, Germany), and light microscopy (Axio 7 observer, Carl Zeiss GmbH, Munich, Germany). CNTs were dispersed and gelled using a Branson Digital Sonifier ultrasonic probe (Wattage 400 W, Branson Ultraschall GmbH, Fürth, Germany). Wet gels were dried in a drying furnace (Heraeus Oven, Thermo Fisher Scientific GmbH, Dreieich, Germany) or in a freeze-dryer (Alpha 1-2LDplus, Martin Christ GmbH, Osterode am Harz, Germany). Monolith characterization was carried out using a Gemini VII surface analyzer (Micromeritics GmbH, Unterschleißheim, Germany), and a Z2.5 tensile strength testing machine (ZwickRoell GmbH, Fürstenfeld, Germany). To measure electrical conductivity, the monoliths were clamped in a 3D printed rig pictured in Figure S1 and contacted by two-point gold pins. Electrochemical experiments were conducted using a Gamry I 1000 E potentiostat (Gamry Instruments, Warminster, PA, USA). For all electrochemical experiments, an asymmetrical two-electrode setup was used. Planar monoliths functioned as working electrodes while a porous steel foam (Alantium Europe GmbH, Munich, Germany) with a pore size of 450 µm was utilized as a counter electrode (see Figure S2). The electrodes were placed parallel in a self-printed test rig (Filament: ABS, Rudolf Wiegand und Partner GmbH, Olching, Germany) (see Figure S2). For potential-controlled adsorption experiments, the amount of adsorbed and desorbed analyte was quantified as triplicates using an Agilent 1100 series high performance liquid chromatography (HPLC) system (Agilent Technologies Inc., Santa Clara, CA, USA).

2.2. Particle Preparation and Characterization

For the determination of the point of zero charge (pHpzc), DI-water was adjusted to pH values from 3 to 10 (pH_{initial}) using 10 mM HCl and NaOH. Afterward, dried CNT and oxCNT particles were weighed to concentrations of 0.005 g L⁻¹, 0.010 g L⁻¹, 0.050 g L⁻¹, and 0.100 g L⁻¹ and added to the liquid media. The suspensions were incubated at 250 rpm and room temperature (RT) for 24 h before measuring the pH again (pH_{final}). All experiments were conducted in triplicates. To study the ultrasonic impact on the gelation of the CNT network, particle concentrations of 10 g L⁻¹ and 40 g L⁻¹ were ultrasonicated (20%, 6 min, 10 s on, 15 s off) while cooled in an ice bath.

2.3. Monolith Synthesis

Our synthesis protocol is derived from the work of Shen et al. [11]. However, changes were made to the existing protocol as we refrained from using SDBS for the dispersion of the CNTs. Instead, the impact of ultrasonication on the dispersion and gelation of the CNT network was studied. We simplified the process with a shortened incubation time for PVA and a subsequent centrifugation step. For the stabilization of the synthesized CNT monoliths, we developed a simple pressing and heat drying approach. In Figure 1, the synthesis steps for the preparation of CNT monoliths are illustrated.

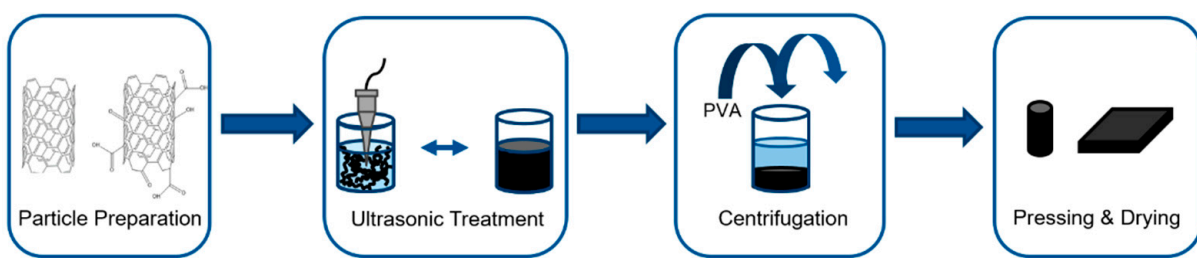


Figure 1. Schematic for the preparation of CNT monoliths.

Wet masses of CNT and oxCNT were dispersed in DI-water. Subsequently, the dispersion was treated ultrasonically for up to 6 min. Afterward, the particles were centrifuged and dispersed in an aqueous 1 wt-% PVA solution. After an incubation time of approx. 5 min and a final centrifugation step, monoliths were formed from the sediment using self-designed pressing molds (pressing weight: 4 kg) for cylindrical and planar monoliths (see Figure 2). For the pressing of monoliths, CNT wet mass is evenly distributed within the pressing mold in a first step. In a second step, the CNT wet mass is compressed with stamps. After pressing, the wet monoliths were dried in a drying furnace (72 h, 60 °C) or by freeze-drying (-58°C , 0.04 mbar, 48 h). For further monolith characterization and electrochemical experiments, only heat-dried monoliths were utilized.

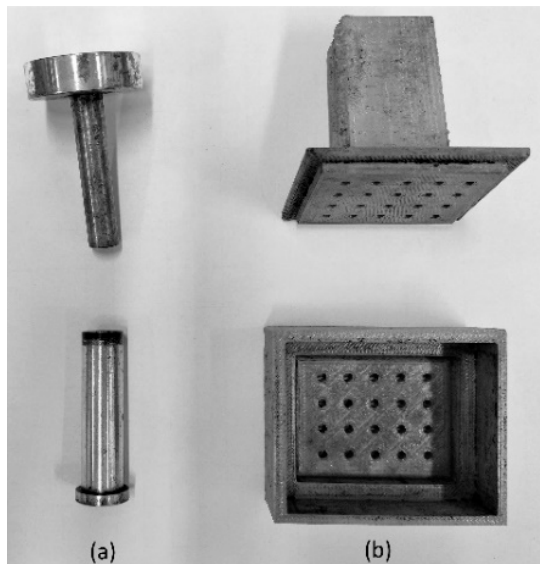


Figure 2. Molds and stamps for the pressing of cylindrical (a) $\varnothing 10\text{ mm}$ and planar monoliths (b) $50 \times 40 \times 5\text{ mm}$.

2.4. Monolith Characterization

The BET surface was determined as triplicates at 77 K under nitrogen atmosphere. By exposing the monoliths to predefined weight loads, the mechanical stability of the monoliths was tested. In addition, tensile strength measurements were conducted for planar monoliths. The conductivity was determined by the two point probe method and determined in analytical and technical triplicates. For electrochemical characterization, the potentiostat was operated in surface mode. As electrolyte solution, 6.5 mL of 5 mM maleic acid adjusted to a pH of 7 was utilized. Chronoamperometric measurements were conducted for up to 300 s in $\pm 100\text{ mV}$ steps. Cyclic voltammetry was conducted 3 consecutive times at a scan rate of 1 mV s^{-1} . The operation range was set between -500 mV and $+500\text{ mV}$ vs. the open circuit potential (OCP).

2.5. Potential-Controlled Adsorption

Maleic acid was utilized as a model analyte. For potential-controlled adsorption experiments, 6.5 mL of 5 mM maleic acid were adjusted to a pH of 7. A potential of +500 mV vs. OCP was applied during the adsorption phase for 15 min. After the adsorption phase, test rig and counter electrode were rinsed and cleaned extensively using DI-water so that only the effect of the working electrode would be observed and no remaining analyte on the test rig and counter electrode could influence the concentration measurement. DI-water at an adjusted pH of 7 was filled into the test rig to recover the model analyte. A potential of −500 mV vs. OCP was applied for 15 min for the desorption phase. Due to its strong UV absorbance maleic acid can easily be detected spectrophotometrically [31,32,36]. Hence, adsorbed and desorbed amounts of maleic acid were determined as triplicates by measuring the concentration in the supernatant through HPLC runs at a wavelength of 258 nm. Electrosorption experiments were conducted for three subsequent runs with washing steps for the monolith and test rig after each run to test the stability of the electrodes.

3. Results

3.1. Particle Oxidation and Characterization

Surface oxidation is often utilized to improve the dispersive behavior and hydrophilicity of CNTs [37,38]. The increased presence of oxygen-containing surface moieties thus leads to enhanced electrostatic repulsion and stabilization of the nanotube dispersion [34]. Intending to synthesize and stabilize monoliths containing minimal quantities of additives, we compared untreated and oxidized CNT particles as raw material prior to monolith synthesis. It therefore has to be considered that oxidation can lead to structural damage and conductivity loss of CNTs [39–41]. Hence, particular focus was given to developing a mild oxidation protocol (30 min, 3:1 *v/v* 3M H₂SO₄ to HNO₃, ratio, 80 °C). As expected, no structural damage could be observed through TEM-imaging for our oxidized nanotubes (see Figure S3). In FTIR measurements, an increase in peak intensity for bands associated with oxygen-containing surface groups indicates the successful surface oxidation of the nanotubes (see Figure S4). As a result of functionalization a dominant increase of C=O stretching vibrations visible at 1118 cm^{−1} proves the augmented presence of ester, ether and alcohol groups on the nanotubes surface [42]. Moreover, an increasing peak intensity for bands associated with C=O stretching can be observed between 1700 cm^{−1} and 1500 cm^{−1} and confirms the presence of carboxylic acid and ketone groups [43]. Thus, we observe functionalization of the nanotubes' surface even upon mild oxidation conditions similar to Avilés et al. [37]. Therefore, we expect good electrical properties of the CNTs.

Further, studying the solid-liquid interface is essential to understanding the later adsorption of charged molecules onto the synthesized monoliths in aqueous systems. In Figure 3, pH-shift experiments for untreated (green) and oxidized (blue, grey) CNTs are presented. An increased number of oxidized surface species for oxCNTs could be proven by determining the point of zero charge (pHpzc). The pHpzc is represented by an intersection with the bisecting line in Figure 3 (pHinitial = pHfinal). For the untreated nanotubes, a pHpzc of 6.56 was determined. In contrast, a pHpzc between 1.67 and 2.16 was observed for the oxidized samples, resulting from the deprotonation of surface hydroxyl groups [44,45]. Thus, the strong influence of the oxidation onto the surface charge and the nanotubes' dispersibility is illustrated. For increasing mass concentrations of oxCNTs, an explicit dependency on the strength of the pH-shift is visible, resulting from the enlarged number and effect of oxidized surface groups. As also reported by Wagner et al. [30] and Trunzer et al. [31], our experiments highlight the remarkable influence of the nanotubes onto aqueous systems due to changes in the EDL.

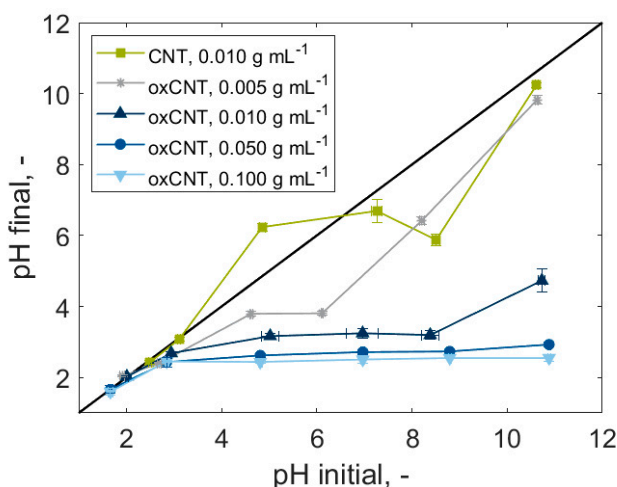


Figure 3. pH-shift experiments for untreated (green) and oxidized CNT-K (blue, grey) particles at differing concentrations. The nanotubes were weighed in as dry mass. Incubation was conducted at RT for 24 h.

3.2. Monolith Stability Dependence on Ultrasonication and Drying

Upon initial dispersion and gelation, carbon aerogels are traditionally dried by supercritical fluid drying or freeze-drying in order to remove the liquid phase without disturbing or collapsing the porous network [46–49]. However, both methods are rather expensive, time-consuming, and hard to handle. With the goal of a simplified and optimized synthesis protocol, we studied the impact of ultrasonication and subsequent heat drying on the monoliths' stability compared to a more traditional dispersant-aided freeze-drying approach. Hereby, we determined ultrasonic treatment prior to pressing and drying of the CNT gel as a critical factor to achieve stable and free-standing monoliths.

Through the high energy impact of sonication onto the CNT suspension and the resulting shear stress, individual agglomerates can be separated, leading to a dispersion of the particles [50,51]. Interestingly, with increasing sonication time, even swelling of the CNT network can be observed, as illustrated in Figure 4a,b. Thus, strong water uptake of the CNT network is indicated, as also discussed by Trunzer et al. [32]. Moreover, with increasing ultrasonic impact, strong gelation of the CNT-water suspension can be triggered. After 6 min of ultrasonic treatment, the CNTs form a gel displaying no free water, as displayed in Figure 4c. However, it has to be considered that similar to harsh oxidation conditions, the high energy impact during ultrasonication can lead to scission and structural damage of the CNTs [50,52,53]. Thus, we additionally studied the impact of sonication-induced shear forces through TEM imaging (see Figure S3), where no significant structural effect on the CNTs could be found upon a six-minute ultrasonic treatment.

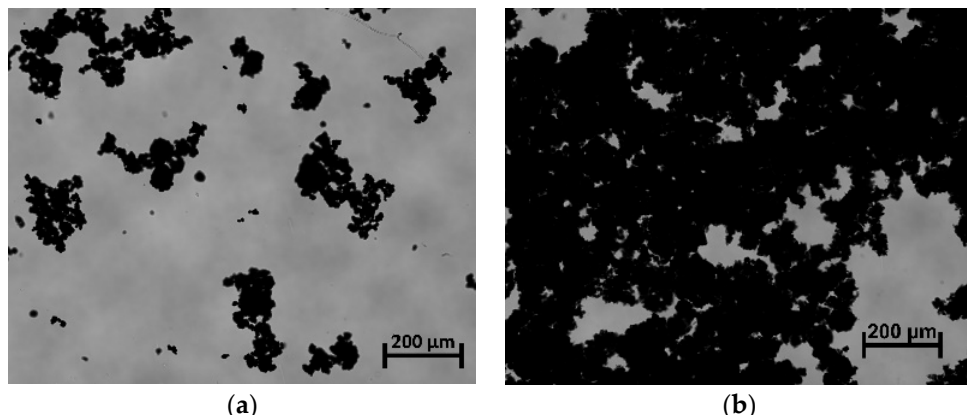


Figure 4. Cont.

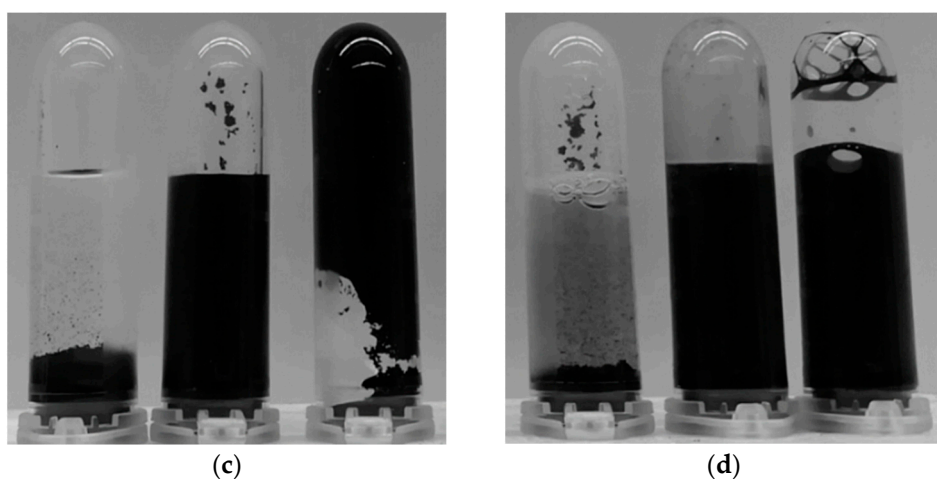


Figure 4. Ultrasonic impact on CNT suspensions: (a) 0.4 g CNTs in 40 mL DI-water, no ultrasonic impact; (b) 0.4 g CNTs in 40 mL DI-water, ultrasonic impact (20%, 6 min, 10 s on, 15 s off) (c) 0.4 g in 40 mL DI-water after different times of US (20%, 10 s on, 15 s off): l.t.r.: 0 min (prompt sedimentation), 3 min (more viscous), 6 min (highly viscous, gel-like); (d) 0.4 g CNTs in 10 mL 10 g L⁻¹ SDBS after different times of US (20%, 10 s on, 15 s off): l.t.r.: 0 min (prompt sedimentation), 3 min (dispersed system), 6 min (dispersed system).

In contrast to an ultrasonically steered approach, the use of dispersing agents has already established itself as a first step in the synthesis of CNT monoliths [11,15–17]. However, utilization of dispersants introduces an additional component to the monoliths' network, further influencing its adsorptive properties, as shown by Li et al. for pristine CNTs [54]. Introducing nanotube gelation through ultrasound, the addition of surfactants disturbed the gelation process in our system (see Figure 4d). Here, the utilized dispersant SDBS strongly accumulated on the surface of the nanotubes during ultrasonication, leading to sterical separation and inhibition of gel formation (see Figure S3d) [55,56]. Consequently, we were able to proceed with our synthesis without additional dispersing agents.

Heat drying the sonicated and pressed CNT-gel, we found that the resulting monoliths remained intact with increasing sonication time even after prolonged water incubation and shaking of the sample container (see Figure 5a). For instance, upon a heat drying approach, the synthesized monoliths showed no sign of disintegration in DI-water even after 6 months of incubation. In contrast, monoliths pressed with no prior sonication treatment dissolved and broke easily upon contact with water. For heat-dried monoliths, a considerable shrinking could be observed during drying as water evaporates from the particle network. Comparison of heat drying to a traditional freeze-drying approach as described by Bryning et al. [17] showed that the initial size of the wet gel is preserved for the most part (see Figure 5b). However, the stability of the monoliths decreases to a great extent as the particle network could not be further stabilized during drying.

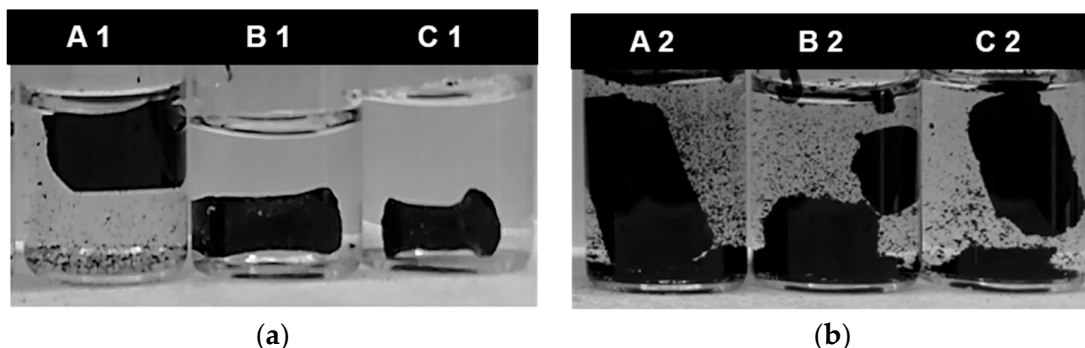


Figure 5. Solubility of cylindrical monoliths in DI-water synthesized with different US duration (A: 0 min, B: 3 min, C: 6 min), dried at 60 °C for 72 h (a) (A1–C1), and freeze-dried for 48 h (b) (A2–C2). Pictures were taken after 1 min of incubation.

3.3. Monolith Structure and Conductivity

For the further characterization of CNT monoliths, PVA was applied as a structural reinforcement as previously described by Bryning et al. [17]. Especially for planar monoliths, utilized for electrosorption and described in Section 3.4, we found that small concentrations of PVA further increased the homogeneity and stability. In the following, we characterize monoliths comprised of untreated and oxidized CNTs to determine their suitability as electrodes in an electrosorption process.

Our synthesized cylindrical monoliths were free-standing and characterized by a remarkably high structural stability. For example, three monoliths with a density of approximately 0.3 g cm^{-3} supported a counterweight of 3000 g (see Figure S5), which roughly translates to over 5000 times their weight. Moreover, the tensile strength for planar monoliths was determined to $4.28 \pm 0.71 \text{ MPa}$, further emphasizing the high structural stability of our CNT monoliths and their suitability as technical electrodes.

The surface area of the untreated nanotubes was determined to $181 \pm 2 \text{ m}^2 \text{ g}^{-1}$. In this context, Trunzer et al. reported a predominance of structurally closed tube ends for the used CNTs, possibly due to the synthesis process [31,57]. Given that, the oxidation of the CNTs did not influence the tube structure as a specific surface area (SSA) of $175 \pm 2 \text{ m}^2 \text{ g}^{-1}$ was measured for the oxidized sample (see Figure 6). Remarkably, the SSA could be preserved during monolith synthesis with untreated and oxidized nanotubes, as the SSA decreased only by 2%, respectively. This effect can be attributed to our additive-free gelation approach and the scarce utilization of PVA as a binder. Within the development of our synthesis protocol, we changed the incubation conditions of the wet gel in 1 wt-% PVA from several days as described by Bryning et al. [17] to a quick dispersion and centrifugation step with subsequent discard of the supernatant. Thus, we expect less PVA accumulation on the surface of the nanotubes, and therefore preservation of the CNTs' electrical and structural properties. Indeed, we were able to synthesize CNT monoliths with a reduced SSA loss compared to similar synthesis approaches [11,24]. For instance, Shen et al. [11] reported an SSA loss of 26% upon monolith synthesis. Hence, with our synthesis protocol, a vast number of possible binding sites for the later application as an electrode in an electrosorption process should be provided, which will be examined and discussed in Section 3.4.

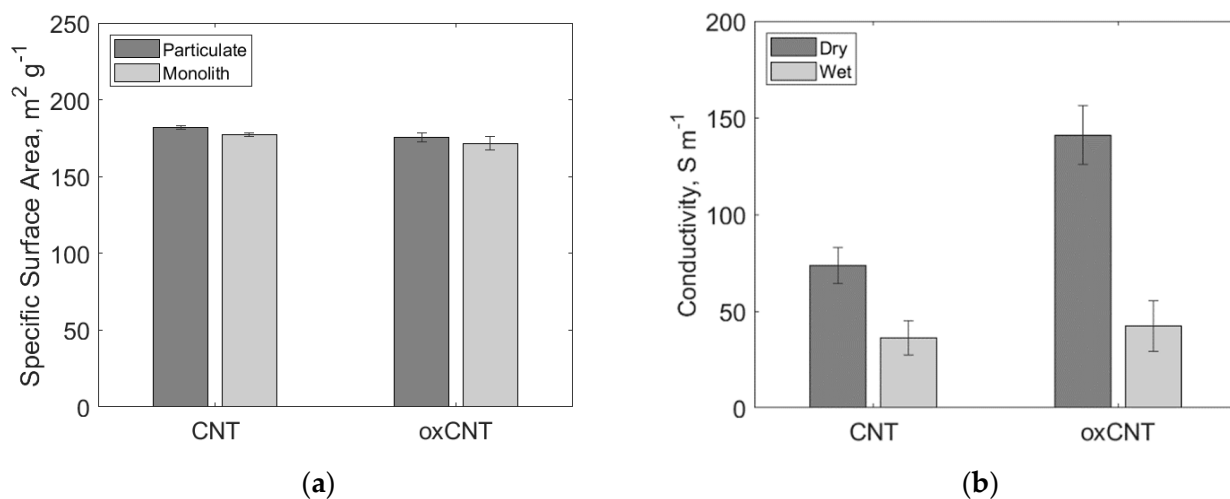


Figure 6. Specific surface area (a) and electrical conductivity (b) for untreated and oxidized monoliths.

Additionally, we observed the preservation of the CNTs' exciting properties through conductivity measurements illustrated in Figure 6b. The electrical conductivity was found to be strongly dependent on the pretreatment of the nanotubes. For untreated monoliths, a conductivity of $74 \pm 9 \text{ S m}^{-1}$ was measured in a dried state. Utilizing monoliths comprised of oxidized nanotubes, the conductivity is almost doubled to $141 \pm 15 \text{ S m}^{-1}$. This indicates an improved particle network formation during the monolith synthesis of the mildly

oxidized nanotubes. After incubation in DI-water, both materials experience a considerable reduction of conductivity. Here, DI-water is stored in the porous structure of the monoliths and inhibits the current flow. Monoliths made of untreated CNTs display a loss of conductivity of 51% to $36 \pm 9 \text{ S m}^{-1}$, while the oxidized monoliths possess a marginally higher conductivity of $42 \pm 13 \text{ S m}^{-1}$. Nonetheless, a high conductivity can be observed for the synthesized monoliths, in a dry and wet state, which is essential for the later electrosorption in aqueous systems. Compared to Shen et al. [11] and Bryning et al. [17], on whom our synthesis protocol builds, we were able to increase the conductivity of MWCNT monoliths by at least one order of magnitude. Here, the pressing and subsequent heat drying of the gelled CNTs might additionally benefit the later conductivity of the resulting monoliths as the particle network becomes more compressed in the process. Simultaneously, we were able to reduce the synthesis steps, as well as the needed equipment and time. Thus, the synthesis and processing costs of the monoliths can be reduced.

3.4. Electrochemical Characterization

Chronoamperometry and cyclic voltammetry (CV) experiments were performed to investigate the suitability for potential-controlled adsorption as well as the electrochemical reactions between the monoliths' surface and the electrolyte environment. Within this framework, maleic acid as a negatively charged electrolyte and target molecule is frequently studied for electrosorption onto carbon electrodes [30–32,36,58]. Brammen et al. [36] and Trunzer et al. [31] already observed reversible maleic acid binding onto a particulate CNT electrode in aqueous systems, thus ensuring its suitability to study the surface-liquid interface of our novel monolithic CNT electrodes.

Figure 7a,b show an initial high current due to the electrodes' double-layer charging. As the double layer extends, the current profile declines until a nearly constant value is achieved. The curves do not reach zero. Hence, a remaining faradaic current is observed for untreated and oxidized monoliths, confirming deviations from an ideal capacitive system. Consequently, the studied monolithic electrodes display a resistance, which can be related to the observed faradaic current. This observed equilibrium current is generated by redox reactions causing constant electron flow on the electrode and is illustrated in Figure 7c. Hereby, an increased current response for monoliths comprised of oxidized CNTs is visible compared to untreated CNT monoliths. The higher faradaic current results from redox reactions between functional groups on the surface of the oxidized nanotubes [59,60]. This assumption can be further confirmed regarding the measured cyclic voltammograms of untreated and oxidized CNT monoliths in Figure 8. As the successive scans remain nearly congruent, no irreversible reactions are expected for the untreated CNTs. Moreover, its smooth shape approximates a capacitive behavior. Monoliths consisting of oxCNTs, on the other hand, behave slightly differently. A greater CV area can be observed, indicating an enlarged capacitance. At around $+550 \text{ mV}$, a redox peak is passed through, assigned to oxidized groups on the monolith's surface. Moreover, the voltammetry scans for oxCNT monoliths pictured in Figure 8 behave slightly inconsistent. Thus, further irreversible reactions on the surface-electrolyte-interface might be displayed. While the increased current response of oxCNT demonstrates improved electrosorption capability, indicated irreversible reactions might negatively impact a reversible process. The following section examines how these interrelationships are manifested in a practical electrosorption process.

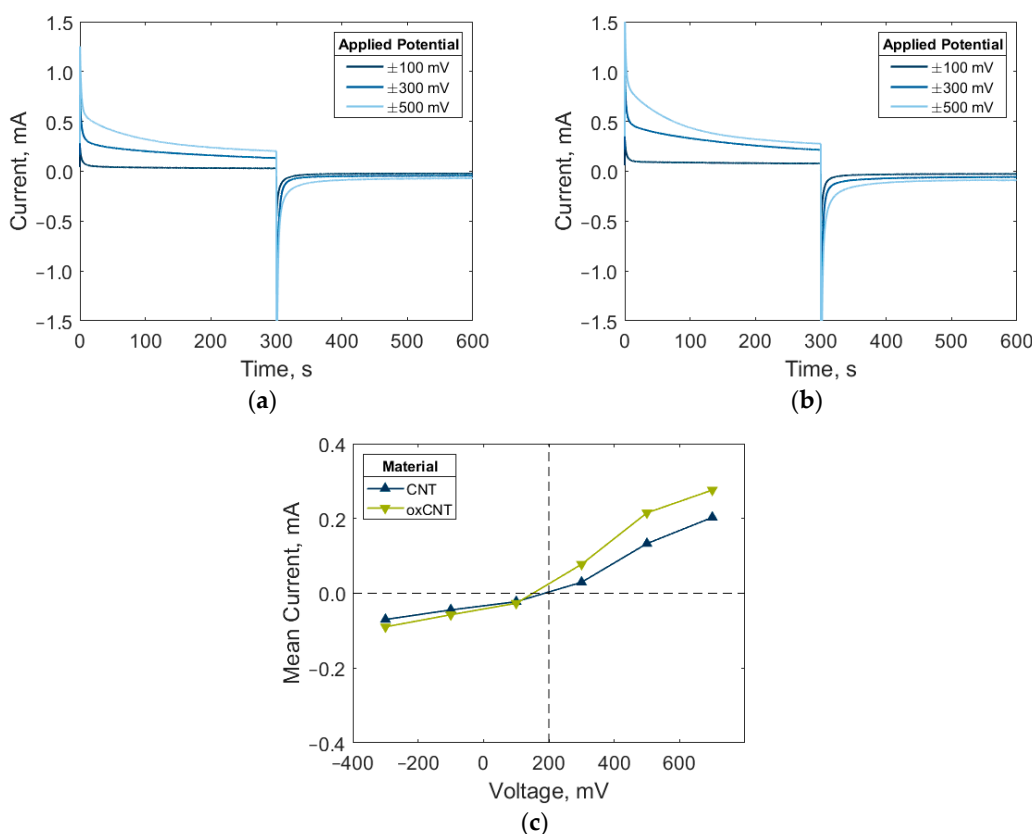


Figure 7. Chronoamperometry experiments for untreated (a) and oxidized (b) CNT-K monoliths. The calculated resulting mean current after EDL rearrangement for both materials is presented in (c).

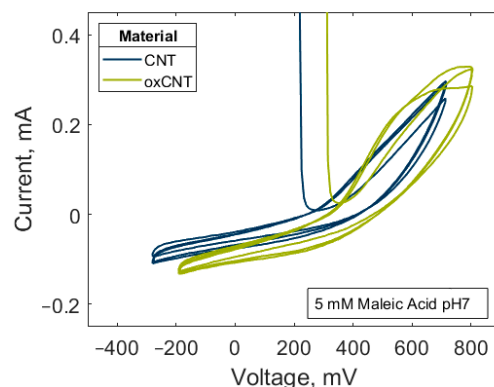


Figure 8. Cyclic voltammetry of untreated and oxidized CNT-K monoliths.

3.5. Potential-Controlled Adsorption on CNT-Monoliths

As a proof of concept, we studied the effect of applied potential on a model analyte's adsorption and desorption behavior, pictured in Figure 9. In potential step experiments, the potential-controlled adsorption behavior onto CNT monoliths could be proven. Untreated CNT monoliths showed initial adsorption of $10.7 \pm 4.7 \mu\text{mol g}^{-1}$. Upon potential switch, a released amount of $6.2 \pm 0.6 \mu\text{mol g}^{-1}$ could be detected, resulting in a release efficiency of 57%. In the following runs, the amount of adsorbed maleic acid firmly declined for the untreated monoliths. Changes on the monolith's surface and strongly bound analyte, not removed through the washing steps, might impair the repeated use of the electrodes and can lead to deviations of the measured concentrations. The availability of active binding sites is thereby drastically reduced. The released amount of analyte slightly increases

during the subsequent runs. The presence of unremoved analyte from the first run is thus confirmed.

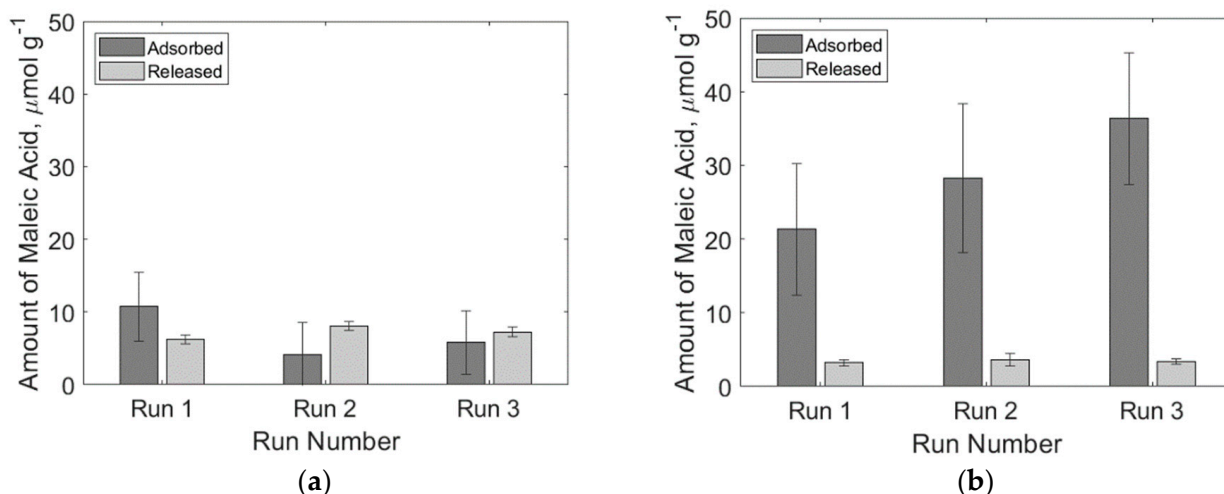


Figure 9. Potential-controlled adsorption and release experiments for 5 mM maleic acid at pH 7 onto untreated (a) and oxidized (b) CNT-K monoliths. A potential of +500 mV for the adsorption and −500 mV for the desorption phase was applied for all experiments. Potentials were applied for 15 min during adsorption and release phase.

A major increase in adsorption capacity can be observed during all runs for oxidized monoliths, possibly due to an enlarged number of binding sites and enhanced current response. However, as the amount of released analyte upon potential inversion is reduced, another binding mechanism between the electrode's oxidized surface and the analyte might be revealed. This heterogeneity is often recognized for carbon nanotubes, as different sorption mechanisms, such as π - π bonds, hydrophobic interactions and hydrogen bonds, may act simultaneously [61]. Particularly for monoliths consisting of oxidized CNTs, electrosorption does not take place exclusively on the surface, aggravating the potential-dependent release of the analyte.

Conventional electrosorption processes studied for the adsorption of smaller inorganic ions show similar adsorption capacities compared to our oxidized monoliths [62–64]. However, it has to be considered that the cited studies were conducted in flow-through setups, thus benefiting from an increased mass transport towards the electrode. In this context, the tested monoliths display good electrosorption properties even at weak applied potentials due to their high conductivity and SSA. Nonetheless, further investigation of the monoliths in a flow-through setup might improve the adsorption and desorption behavior due to mass transport effects.

4. Conclusions and Outlook

This study presents a simple and cost-efficient synthesis protocol, preserving the outstanding structural and electrical properties of carbon nanotubes during monolith synthesis and leading to stable and free-standing monoliths. Moreover, our work combines a broad material characterization of the synthesized monoliths with a subsequent investigation of interfacial effects occurring on the monoliths' surface, as well as an integrated electrosorption study. Thus, it paves the way towards a future application of monolithic CNT electrodes in an electrochemically driven separation process.

For the stability of the synthesized monoliths, we determined the dispersion and gelation of the particles by ultrasonication during the synthesis process to be a key factor. Thus, ultrasonic treatment led to strong gelation as drying in a heating chamber further stabilized the CNT network. We utilized untreated and mildly oxidized CNTs for monolith synthesis. Both materials enable the formation of stable monoliths with a comparable specific surface area. However, by using oxidized CNTs the conductivity of the monoliths

could be strongly increased, indicating a more homogenous and pronounced particle network. Upon electrochemical characterization, the presence of capacitive and faradaic currents could be determined for both materials. However, pronounced faradaic currents were detected with oxidized monoliths, leading to an overall stronger current response. The potential-controlled adsorption of maleic acid was investigated as a proof of concept for an electrosorption process on CNT monoliths. Untreated and oxidized monoliths showed electrosorption behavior. While the adsorption capacity could be improved through oxidation, strong heterogeneous interactions still complicate a potential-triggered release of the model analyte. In this respect, the utilization of electro-active composites might be a possible way to control the reversible electrosorption onto CNT monoliths. Furthermore, the interfacial interactions guiding the reversible electrosorption of organic molecules should be further examined. With the goal of developing a potential-controlled process for biotechnological separations, we continue working on a preparative setup for the targeted electrosorption onto CNT monolith electrodes.

Supplementary Materials: The following are available online at <https://www.mdpi.com/article/10.3390/app11209390/s1>, Figure S1: Test rig for conductivity measurements on cylindrical monoliths. Figure S2: Electrode contacting and test rig for potential-controlled adsorption experiments. Figure S3: Agglomerates of CNTs after oxidative and ultrasonic treatment in DI-Water and SDBS. Figure S4: FTIR spectra of untreated and oxidized CNT-K particles. Figure S5: Mechanical strength of cylindrical and planar monoliths.

Author Contributions: T.T., P.F.-G. and S.B. designed the project, D.R., T.T., J.H., J.R., performed the experiments. All authors assisted in evaluating the results. D.R. wrote the manuscript. T.T., P.F.-G. and S.B. assisted in reviewing and editing the manuscript. Financial acquisition and project administration by P.F.-G. and S.B. All authors have read and agreed to the published version of the manuscript.

Funding: The research was funded by the Federal Ministry of Education and Research under the name S3kapel (grant number 13XP5038A). This work was supported by the Technical University of Munich (TUM) through the TUM Open Access Publishing Fund.

Institutional Review Board Statement: Not applicable.

Informed Consent Statement: Not applicable.

Data Availability Statement: The original data related to this research can be asked at any time to the corresponding author's email: d.roecker@tum.de.

Acknowledgments: We thank Sebastian Schwaminger and Chiara Turrina for the support and advice regarding TEM imaging. In addition, we thank Tim Mader for his assistance in the laboratory. Moreover, we want to thank several groups of the TUM for their support and the use of their equipment: the Institute for Machine Tools and Industrial Management for their assistance regarding the 3D printing of the setup and the pressing molds; the Chair of Medical Materials and Implants for the support in tensile testing of the monoliths and the Associate Professorship of Electron Microscopy for TEM imaging.

Conflicts of Interest: The authors declare no conflict of interest. The funders had no role in the design of the study; in the collection, analyses, or interpretation of data; in the writing of the manuscript, or in the decision to publish the results.

References

1. Iijima, S. Helical microtubules of graphitic carbon. *Nature* **1991**, *354*, 56–58. [[CrossRef](#)]
2. Ebbesen, T.W.; Lezec, H.J.; Hiura, H.; Bennett, J.W.; Ghaemi, H.F.; Thio, T. Electrical conductivity of individual carbon nanotubes. *Nat. Cell Biol.* **1996**, *382*, 54–56. [[CrossRef](#)]
3. Pop, E.; Mann, D.; Wang, Q.; Goodson, K.; Dai, H. Thermal conductance of an individual single-wall carbon nanotube above room temperature. *Nano Lett.* **2006**, *6*, 96–100. [[CrossRef](#)] [[PubMed](#)]
4. Treacy, M.M.J.; Ebbesen, T.W.; Gibson, J.M. Exceptionally high Young's modulus observed for individual carbon nanotubes. *Nat. Cell Biol.* **1996**, *381*, 678–680. [[CrossRef](#)]
5. Evanoff, K.; Khan, J.; Balandin, A.A.; Magasinski, A.; Ready, W.J.; Fuller, T.F.; Yushin, G. Towards ultrathick battery electrodes: Aligned carbon nanotube-enabled architecture. *Adv. Mater.* **2012**, *24*, 533–537. [[CrossRef](#)] [[PubMed](#)]

6. Sotowa, C.; Origgi, G.; Takeuchi, M.; Nishimura, Y.; Takeuchi, K.; Jang, I.Y.; Kim, Y.J.; Hayashi, T.; Kim, Y.A.; Endo, M.; et al. The reinforcing effect of combined carbon nanotubes and acetylene blacks on the positive electrode of lithium-ion batteries. *ChemSusChem* **2008**, *1*, 911–915. [CrossRef] [PubMed]
7. De Volder, M.F.L.; Tawfick, S.; Baughman, R.H.; Hart, A.J. Carbon nanotubes: Present and future commercial applications. *Science* **2013**, *339*, 535–539. [CrossRef]
8. Park, M.-Y.; Kim, C.-G.; Kim, J.-H. CNT-coated quartz woven fabric electrodes for robust lithium-ion structural batteries. *Appl. Sci.* **2020**, *10*, 8622. [CrossRef]
9. Comba, F.N.; Romero, M.R.; Garay, F.S.; Baruzzi, A.M. Mucin and carbon nanotube-based biosensor for detection of glucose in human plasma. *Anal. Biochem.* **2018**, *550*, 34–40. [CrossRef]
10. Cai, H.; Cao, X.; Jiang, Y.; He, P.; Fang, Y. Carbon nanotube-enhanced electrochemical DNA biosensor for DNA hybridization detection. *Anal. Bioanal. Chem.* **2003**, *375*, 287–293. [CrossRef]
11. Shen, Y.; Du, A.; Wu, X.-L.; Li, X.-G.; Shen, J.; Zhou, B. Low-cost carbon nanotube aerogels with varying and controllable density. *J. Sol Gel Sci. Technol.* **2016**, *79*, 76–82. [CrossRef]
12. Kohlmeyer, R.R.; Loh, M.; Deng, J.; Liu, H.; Chen, J. Preparation of stable carbon nanotube aerogels with high electrical conductivity and porosity. *Carbon* **2011**, *49*, 2352–2361. [CrossRef]
13. Zou, J.; Liu, J.; Karakoti, A.; Kumar, A.; Joung, D.; Li, Q.; Khondaker, S.I.; Seal, S.; Zhai, L. Ultralight multiwalled carbon nanotube aerogel. *ACS Nano* **2010**, *4*, 7293–7302. [CrossRef] [PubMed]
14. You, B.; Wang, L.; Yao, L.; Yang, J. Threedimensional N-doped graphene–CNT networks for supercapacitor. *Chem. Commun.* **2013**, *49*, 5016–5018. [CrossRef]
15. Haghgoo, M.; Yousefi, A.A.; Mehr, M.J.Z.; Celzard, A.; Fierro, V.; Léonard, A.; Job, N. Characterization of multi-walled carbon nanotube dispersion in resorcinol–formaldehyde aerogels. *Microporous Mesoporous Mater.* **2014**, *184*, 97–104. [CrossRef]
16. Du, R.; Zhao, Q.; Zhang, N.; Zhang, J. Macroscopic carbon nanotube-based 3D monoliths. *Small* **2015**, *11*, 3263–3289. [CrossRef]
17. Bryning, M.B.; Milkie, D.E.; Islam, M.; Hough, L.A.; Kikkawa, J.M.; Yodh, A.G. Carbon nanotube aerogels. *Adv. Mater.* **2007**, *19*, 661–664. [CrossRef]
18. Zhang, X.; Liu, J.; Xu, B.; Su, Y.; Luo, Y. Ultralight conducting polymer/carbon nanotube composite aerogels. *Carbon* **2011**, *49*, 1884–1893. [CrossRef]
19. Du, R.; Zhang, N.; Xu, H.; Mao, N.; Duan, W.; Wang, J.; Zhao, Q.; Liu, Z.; Zhang, J. CMP aerogels: Ultrahigh-surface-area carbon-based monolithic materials with superb sorption performance. *Adv. Mater.* **2014**, *26*, 8053–8058. [CrossRef]
20. Maghfirah, A.; Yudianti, R.; Sinuhaji, P.; Hutabarat, L.G. Preparation of poly(vinyl) alcohol—Multiwalled carbon nanotubes nanocomposite as conductive and transparent film using casting method. *J. Phys. Conf. Ser.* **2018**, *1116*, 032017. [CrossRef]
21. Singh, R.; Singh, M.; Bhartiya, S.; Singh, A.; Kohli, D.; Ghosh, P.C.; Meenakshi, S.; Gupta, P. Facile synthesis of highly conducting and mesoporous carbon aerogel as platinum support for PEM fuel cells. *Int. J. Hydrog. Energy* **2017**, *42*, 11110–11117. [CrossRef]
22. Chen, W.; Rakhi, R.B.; Alshareef, H.N. High energy density supercapacitors using macroporous kitchen sponges. *J. Mater. Chem.* **2012**, *22*, 14394–14402. [CrossRef]
23. Li, Y.; Kang, Z.; Yan, X.; Cao, S.; Li, M.; Guo, Y.; Huan, Y.; Wen, X.; Zhang, Y. A three-dimensional reticulate CNT-aerogel for a high mechanical flexibility fiber supercapacitor. *Nanoscale* **2018**, *10*, 9360–9368. [CrossRef]
24. Zhou, Y.; Hu, X.; Guo, S.; Yu, C.; Zhong, S.; Liu, X. Multi-functional graphene/carbon nanotube aerogels for its applications in supercapacitor and direct methanol fuel cell. *Electrochim. Acta* **2018**, *264*, 12–19. [CrossRef]
25. Tesfaye, R.M.; Das, G.; Park, B.J.; Kim, J.; Yoon, H.H. Ni-Co bimetal decorated carbon nanotube aerogel as an efficient anode catalyst in urea fuel cells. *Sci. Rep.* **2019**, *9*, 1–9. [CrossRef] [PubMed]
26. Du, R.; Zhang, N.; Zhu, J.; Wang, Y.; Xu, C.; Hu, Y.; Mao, N.; Xu, H.; Duan, W.; Zhuang, L.; et al. Nitrogen-doped carbon nanotube aerogels for high-performance ORR catalysts. *Small* **2015**, *11*, 3903–3908. [CrossRef] [PubMed]
27. Biesheuvel, P.M.; Porada, S.; Levi, M.; Bazant, M. Attractive forces in microporous carbon electrodes for capacitive deionization. *J. Solid State Electrochem.* **2014**, *18*, 1365–1376. [CrossRef]
28. Wang, L.; Wang, M.; Huang, Z.-H.; Cui, T.; Gui, X.; Kang, F.; Wang, K.; Wu, D. Capacitive deionization of NaCl solutions using carbon nanotube sponge electrodes. *J. Mater. Chem.* **2011**, *21*, 18295–18299. [CrossRef]
29. Wang, X.Z.; Li, M.G.; Chen, Y.W.; Cheng, R.M.; Huang, S.M.; Pan, L.K.; Sun, Z. Electrosorption of NaCl solutions with carbon nanotubes and nanofibers composite film electrodes. *Electrochim. Solid State Lett.* **2006**, *9*, e23–e26. [CrossRef]
30. Wagner, R.; Bag, S.; Trunzer, T.; Fraga-García, P.; Wenzel, W.; Berensmeier, S.; Franzreb, M. Adsorption of organic molecules on carbon surfaces: Experimental data and molecular dynamics simulation considering multiple protonation states. *J. Colloid Interface Sci.* **2021**, *589*, 424–437. [CrossRef]
31. Trunzer, T.; Stummvoll, T.; Porzenheim, M.; Fraga-García, P.; Berensmeier, S. A carbon nanotube packed bed electrode for small molecule electrosorption: An electrochemical and chromatographic approach for process description. *Appl. Sci.* **2020**, *10*, 1133. [CrossRef]
32. Trunzer, T.; Fraga-García, P.; Tschuschner, M.-P.A.; Voltmer, D.; Berensmeier, S. The electrosorptive response of a carbon nanotube flow-through electrode in aqueous systems. *Chem. Eng. J.* **2022**, *428*, 13100. [CrossRef]
33. Moraes, R.A.; De Matos, C.F.; Castro, E.G.; Schreiner, W.H.; Oliveira, M.M.; Zarbin, A.J.G. The effect of different chemical treatments on the structure and stability of aqueous dispersion of iron- and iron oxide-filled multi-walled carbon nanotubes. *J. Braz. Chem. Soc.* **2011**, *22*, 2191–2201. [CrossRef]

34. Shaffer, M.; Fan, X.; Windle, A. Dispersion and packing of carbon nanotubes. *Carbon* **1998**, *36*, 1603–1612. [[CrossRef](#)]
35. Vigolo, B.; Pénicaud, A.; Coulon, C.; Sauder, C.; Pailler, R.; Journet, C.; Bernier, P.; Poulin, P. Macroscopic fibers and ribbons of oriented carbon nanotubes. *Science* **2000**, *290*, 1331–1334. [[CrossRef](#)] [[PubMed](#)]
36. Brammen, M.; Fraga-García, P.; Berensmeier, S. Carbon nanotubes-A resin for electrochemically modulated liquid chromatography. *J. Sep. Sci.* **2017**, *40*, 1176–1183. [[CrossRef](#)] [[PubMed](#)]
37. Avilés, F.; Cauch-Rodríguez, J.; Moo-Tah, L.; May-Pat, A.; Vargas-Coronado, R.F. Evaluation of mild acid oxidation treatments for MWCNT functionalization. *Carbon* **2009**, *47*, 2970–2975. [[CrossRef](#)]
38. Farbod, M.; Tadavani, S.K.; Kiasat, A. Surface oxidation and effect of electric field on dispersion and colloids stability of multiwalled carbon nanotubes. *Colloids Surf. A Physicochem. Eng. Asp.* **2011**, *384*, 685–690. [[CrossRef](#)]
39. Wepasnick, K.A.; Smith, B.A.; Schrote, K.E.; Wilson, H.K.; Diegelmann, S.R.; Fairbrother, D.H. Surface and structural characterization of multi-walled carbon nanotubes following different oxidative treatments. *Carbon* **2011**, *49*, 24–36. [[CrossRef](#)]
40. Kim, Y.-T.; Mitani, T. Competitive effect of carbon nanotubes oxidation on aqueous EDLC performance: Balancing hydrophilicity and conductivity. *J. Power Sour.* **2006**, *158*, 1517–1522. [[CrossRef](#)]
41. Schwaminger, S.P.; Brammen, M.W.; Zunhammer, F.; Däumler, N.; Fraga-García, P.; Berensmeier, S. Iron oxide nanoparticles: Multiwall carbon nanotube composite materials for batch or chromatographic biomolecule separation. *Nanoscale Res. Lett.* **2021**, *16*, 1–10. [[CrossRef](#)]
42. Țucureanu, V.; Matei, A.; Avram, M.A. FTIR spectroscopy for carbon family study. *Crit. Rev. Anal. Chem.* **2016**, *46*, 502–520. [[CrossRef](#)]
43. Stobinski, L.; Lesiak, B.; Kövér, L.; Tóth, J.; Biniak, S.; Trykowski, G.; Judek, J. Multiwall carbon nanotubes purification and oxidation by nitric acid studied by the FTIR and electron spectroscopy methods. *J. Alloy. Compd.* **2010**, *501*, 77–84. [[CrossRef](#)]
44. Morales-Torres, S.; Silva, T.L.S.; Pastrana-Martínez, L.M.; Brandão, A.T.S.C.; Figueiredo, J.L.; Silva, A.M.T. Modification of the surface chemistry of single- and multi-walled carbon nanotubes by HNO_3 and H_2SO_4 hydrothermal oxidation for application in direct contact membrane distillation. *Phys. Chem. Chem. Phys.* **2014**, *16*, 12237–12250. [[CrossRef](#)]
45. Gatabi, M.P.; Moghaddam, H.M.; Ghorbani, M. Point of zero charge of maghemite decorated multiwalled carbon nanotubes fabricated by chemical precipitation method. *J. Mol. Liq.* **2016**, *216*, 117–125. [[CrossRef](#)]
46. Fu, R.; Zheng, B.; Liu, J.; Dresselhaus, M.S.; Dresselhaus, G.; Satcher, J.H.; Baumann, T.F. The fabrication and characterization of carbon aerogels by gelation and supercritical drying in isopropanol. *Adv. Funct. Mater.* **2003**, *13*, 558–562. [[CrossRef](#)]
47. Pekala, R.W.; Farmer, J.C.; Alviso, C.T.; Tran, T.D.; Mayer, S.T.; Miller, J.M.; Dunn, B. Carbon aerogels for electrochemical applications. *J. Non Cryst. Solids* **1998**, *225*, 74–80. [[CrossRef](#)]
48. Tamon, H.; Ishizaka, H.; Yamamoto, T.; Suzuki, T. Influence of freeze-drying conditions on the mesoporosity of organic gels as carbon precursors. *Carbon* **2000**, *38*, 1099–1105. [[CrossRef](#)]
49. Thongprachan, N.; Nakagawa, K.; Sano, N.; Charinpanitkul, T.; Tanthapanichakoon, W. Preparation of macroporous solid foam from multi-walled carbon nanotubes by freeze-drying technique. *Mater. Chem. Phys.* **2008**, *112*, 262–269. [[CrossRef](#)]
50. Huang, Y.Y.; Knowles, T.P.J.; Terentjev, E.M. Strength of nanotubes, filaments, and nanowires from sonication-induced scission. *Adv. Mater.* **2009**, *21*, 3945–3948. [[CrossRef](#)]
51. Yamamoto, T.; Miyauchi, Y.; Motoyanagi, J.; Fukushima, T.; Aida, T.; Kato, M.; Maruyama, S. Improved bath sonication method for dispersion of individual single-walled carbon nanotubes using new triphenylene-based surfactant. *Jpn. J. Appl. Phys.* **2008**, *47*, 2000–2004. [[CrossRef](#)]
52. Park, H.J.; Park, M.; Chang, J.Y.; Lee, H. The effect of pre-treatment methods on morphology and size distribution of multi-walled carbon nanotubes. *Nanotechnology* **2008**, *19*, 335702. [[CrossRef](#)]
53. Huang, Y.Y.; Terentjev, E.M. Dispersion of carbon nanotubes: Mixing, sonication, stabilization, and composite properties. *Polymers* **2012**, *4*, 275–295. [[CrossRef](#)]
54. Li, H.; Wei, C.; Zhang, D.; Pan, B. Adsorption of bisphenol A on dispersed carbon nanotubes: Role of different dispersing agents. *Sci. Total. Environ.* **2019**, *655*, 807–813. [[CrossRef](#)]
55. Niyogi, S.; Boukhalfa, S.; Chikkannanavar, S.B.; McDonald, T.J.; Heben, A.M.J.; Doorn, S.K. Selective aggregation of single-walled carbon nanotubes via salt addition. *J. Am. Chem. Soc.* **2007**, *129*, 1898–1899. [[CrossRef](#)]
56. Clark, M.D.; Subramanian, S.; Krishnamoorti, R. Understanding surfactant aided aqueous dispersion of multi-walled carbon nanotubes. *J. Colloid Interface Sci.* **2011**, *354*, 144–151. [[CrossRef](#)] [[PubMed](#)]
57. Frackowiak, E.; Metenier, K.; Bertagna, V.; Beguin, F. Supercapacitor electrodes from multiwalled carbon nanotubes. *Appl. Phys. Lett.* **2000**, *77*, 2421–2423. [[CrossRef](#)]
58. Wagner, R.; Winger, S.; Franzreb, M. Predicting the potential of capacitive deionization for the separation of pH-dependent organic molecules. *Eng. Life Sci.* **2021**, *1*–18. [[CrossRef](#)]
59. Lee, S.W.; Gallant, B.M.; Lee, Y.; Yoshida, N.; Kim, D.Y.; Yamada, Y.; Noda, S.; Yamada, A.; Shao-Horn, Y. Self-standing positive electrodes of oxidized few-walled carbon nanotubes for light-weight and high-power lithium batteries. *Energy Environ. Sci.* **2012**, *5*, 5437–5444. [[CrossRef](#)]
60. Lee, S.W.; Gallant, B.M.; Byon, H.R.; Hammond, P.T.; Shao-Horn, Y. Nanostructured carbon-based electrodes: Bridging the gap between thin-film lithium-ion batteries and electrochemical capacitors. *Energy Environ. Sci.* **2011**, *4*, 1972–1985. [[CrossRef](#)]
61. Pan, B.; Xing, B. Adsorption mechanisms of organic chemicals on carbon nanotubes. *Environ. Sci. Technol.* **2008**, *42*, 9005–9013. [[CrossRef](#)] [[PubMed](#)]

62. Suss, M.E.; Porada, S.; Sun, X.; Biesheuvel, P.M.; Yoon, J.; Presser, V. Water desalination via capacitive deionization: What is it and what can we expect from it? *Energy Environ. Sci.* **2015**, *8*, 2296–2319. [[CrossRef](#)]
63. Peng, Z.; Zhang, D.; Yan, T.; Zhang, J.; Shi, L. Three-dimensional micro/mesoporous carbon composites with carbon nanotube networks for capacitive deionization. *Appl. Surf. Sci.* **2013**, *282*, 965–973. [[CrossRef](#)]
64. Pan, L.; Wang, X.; Gao, Y.; Zhang, Y.; Chen, Y.; Sun, Z. Electrosorption of anions with carbon nanotube and nanofibre composite film electrodes. *Desalination* **2009**, *244*, 139–143. [[CrossRef](#)]